Ultrafast Exciton Dynamics in InGaN/GaN and Rh/Cr 2 O 3 Nanoparticle-Decorated InGaN/GaN Nanowires

ARTICLE *in* JOURNAL OF PHYSICAL CHEMISTRY LETTERS · JUNE 2015

Impact Factor: 7.46 · DOI: 10.1021/acs.jpclett.5b00909

THE JOURNAL OF PHYSICAL CHEMISTRY Letters

Letter

pubs.acs.org/JPCL

Ultrafast Exciton Dynamics in InGaN/GaN and Rh/Cr_2O_3 Nanoparticle-Decorated InGaN/GaN Nanowires

Ying-Chih Pu,[†] M. G. Kibria,[‡] Zetian Mi,*[,‡] and Jin Z. Zhang*[,†]

[†]Department of Chemistry and Biochemistry, University of California, 1156 High Street, Santa Cruz, California 95064, United States

[‡]Department of Electrical and Computer Engineering, McGill University, 3480 University Street, Montreal, Québec H3A 0E9, Canada

Supporting Information

ABSTRACT: Ultrafast exciton and charge-carrier dynamics in InGaN/GaN nanowires (NWs) with and without Rh/Cr_2O_3 nanoparticle (NP) decoration have been investigated using femtosecond transient absorption (TA) techniques with excitation at 415 nm and white-light probe (450−700 nm). By comparing the TA profiles between InGaN/GaN and InGaN/GaN-Rh/Cr_2O_3 NWs, an additional decay component on the medium time scale (~50 ps) was identified with Rh/Cr_2O_3 decoration, which is attributed to interfacial charge transfer from InGaN/GaN NWs to Rh/Cr_2O_3 NPs, desired for light energy conversion applications. This is consistent with reduced photoluminescence (PL) of the NWs by the Rh/Cr_2O_3 NPs. A kinetic model was developed to explain the TA results and gain further insight into the exciton and charge-carrier dynamics.

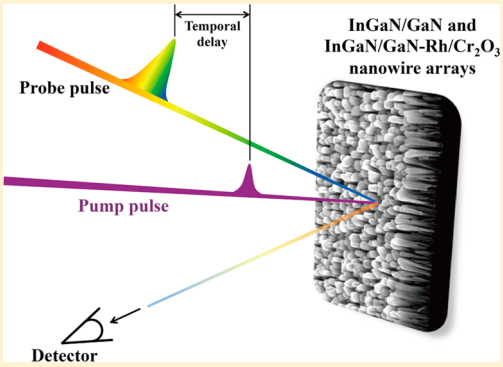

InGaN/GaN NW heterostructures have been intensively studied recently because of their applications in light-emitting diodes (LEDs) and lasers due to their tunable bandgap from UV to near-infrared spectral range.[1−6] One facile method to tune the bandgap is changing the ratio of In:Ga in $In_xGa_{1-x}N$ nanostructures, allowing for significant improvements in the ability to harvest photons from sunlight, which has demonstrated great benefits in solar-to-fuel conversion.[7−13] In addition, the band edges of $In_xGa_{1-x}N$ straddle the reduction and oxidation potentials of water, leading to a thermodynamically favorable band structure for hydrogen and oxygen generation from water splitting.[14] AlOtaibi et al. first reported stable photoelectrochemical (PEC) hydrogen generation by core/shell InGaN/GaN segments in NW arrays,[13] which exhibited a high incident-photon-to-current-conversion efficiency (IPCE) of ~27% as measured under UV and visible-light irradiation. Additionally, 3D core/shell GaN/InGaN nanorod arrays have shown strong activity in visible-light-driven water splitting.[10] Although InGaN/GaN nanostructures are good candidates for use in solar fuel generation, the intrinsic quantum confinement of localized states[15−17] may limit interfacial charge transfer (CT) and thereby the efficiency of photoelectric conversion.[18]

In the meantime, surface modification of semiconductors by noble-metal NP has been found to improve the efficiency of photocatalysis as a result of the enhanced separation of photoexcited charge carriers.[19−22] For instance, well-controlled Pt NPs coated on Si NWs by atomic layer deposition (ALD) showed high solar-to-fuel conversion efficiency.[21,23] In addition, Pt NP-decorated CdSe nanorods exhibiting high photoactivity due to improved charge separation have also been reported.[24] Furthermore, core/shell InGaN/GaN NWs with surface-decorated Rh/Cr_2O_3 NPs (indicated as InGaN/GaN-Rh/Cr_2O_3 hereafter) have also shown efficient photocatalytic water splitting, generating H_2 and O_2 under UV, blue, and green light irradiation.[25] The absorbed photon conversion efficiency of double-band InGaN/GaN-Rh/Cr_2O_3 NWs was estimated to be ~69% at 400−475 nm, which was the highest reported value in the visible spectrum.[26,27] Although metal-decorated semiconductor nanostructures are promising to improve charge separation in photocatalytic energy conversion processes, detailed mechanistic studies are still lacking and needed in order to realize their potential.

Consequently, examination of charge-carrier dynamics in semiconductor nanocomposites is critical. The investigation could assess the correlation between the exciton relaxation processes and performance of solar-to-fuel conversion.[28−32] For example, the ultrafast charge injection rate constant of 1.7×10^{11} s^{-1} from CdSe to TiO_2 was observed in their exciton dynamic investigation because of the unique CdSe/TiO_2 nanorod fabrication method, Oblique Angle Codeposition. This technic resulted in the large interfacial strong coupling area between CdSe and TiO_2 to achieve ultrafast interfacial CT.[33] The dynamic study provided useful information about how to optimize the CdSe/TiO_2 nanorod composite structures for application in solar fuel generation.[34] Likewise, upon the dynamic study of three components TiO_2-Au-CdS, the Au NPs not only served as an electron relay of charge carriers between

Received: May 2, 2015
Accepted: June 12, 2015

DOI: 10.1021/acs.jpclett.5b00909
J. Phys. Chem. Lett. 2015, 6, 2649−2656

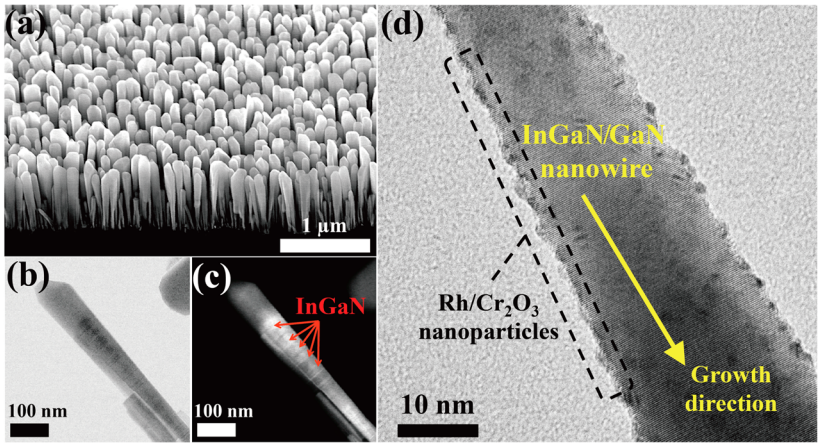

Figure 1. (a) SEM image of as-grown InGaN/GaN NW array on Si (111) substrate. (b) TEM and (c) HAADF images showing five InGaN segments embedded in a GaN NW. (d) HRTEM image of core/shell Rh/Cr_2O_3 nanoparticle-decorated InGaN/GaN NW.

CdS and TiO_2, but also acted as a plasmonic photosensitizer to inject electron into TiO_2 to improve solar-to-chemical energy conversion efficiency.[35] However, to date, there have been no investigations on the charge-carrier dynamics of InGaN/GaN-Rh/Cr_2O_3 NWs and their correlation to solar fuel generation.

In this Letter, we have carried out ultrafast dynamics studies of p-type InGaN/GaN quantum-well (QW) NWs (five InGaN segments, In:Ga 2:8) synthesized by plasma-assisted molecular beam epitaxy (PAMBE). Core/shell Rh/Cr_2O_3 NPs were photodeposited on as-grown InGaN/GaN NWs to form InGaN/GaN-Rh/Cr_2O_3 NW composite structures to better understand the role of core/shell Rh/Cr_2O_3 nanoparticles on the photoactivity of InGaN/GaN NWs. Characterizations of the structural and optical properties of the both samples were accomplished by scanning electron microscopy (SEM), transmission electron microscopy (TEM), and photoluminescence spectroscopy (PL). Ultrafast exciton dynamics of the InGaN/GaN and InGaN/GaN-Rh/Cr_2O_3 NWs was studied by femtosecond pump−probe laser spectroscopy. The obtained dynamics data were fit using mathematic functions and further analyzed with a kinetic model to extract time or rate constants of exciton relaxation. The kinetic modeling results indicate that the Rh/Cr_2O_3 cocatalyst plays a critical role in the medium time scale (~50 ps) for achieving the noteworthy charge separation in InGaN/GaN NWs. This charge-carrier dynamics can be well-correlated to superior performance of the cocatalyst-decorated InGaN/GaN NWs.

The SEM image in Figure 1a shows uniform arrays of as-grown p-type InGaN/GaN multiband NWs on Si (111) substrate with an average height of ~600 nm and diameter of ~40−100 nm. Figure 1b shows a TEM image of a representative InGaN/GaN NW, and Figure 1c shows a high-angle annular dark field (HADDF) image that exhibits atomic contrast between GaN (draker) and InGaN (brighter) segments (each ~30−40 nm). Figure 1d shows a bright-field TEM image of a single InGaN/GaN NW after photodeposition of Rh/Cr_2O_3 NPs, which reveals uniform distribution of Rh/Cr_2O_3 NPs with average particle size around 2−5 nm on the lateral nonpolar surface of InGaN/GaN NW. The detailed characterization of Rh/Cr_2O_3 NPs on the surface of InGaN/GaN NW has been analyzed by the EDX elemental mapping in our previous study.[27]

The PL and PL excitation (PLE) spectra of InGaN/GaN and InGaN/GaN-Rh/Cr_2O_3 NWs are shown in Figure 2. In

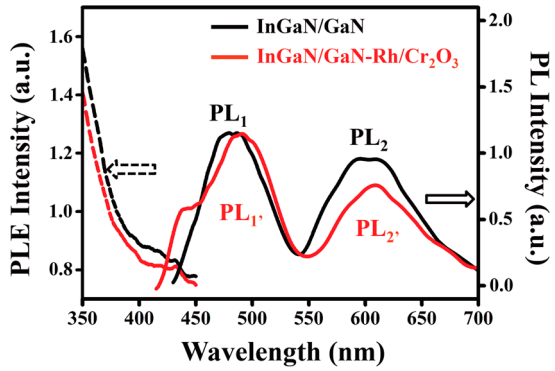

Figure 2. PL (solid line) and PLE (dashed line) spectra of InGaN/GaN and InGaN/GaN-Rh/Cr_2O_3 NWs. (Dashed and solid arrows indicate their PLE and PL spectra, respectively.)

addition, the optical properties of InGaN/GaN and InGaN/GaN-Rh/Cr_2O_3 NWs are summarized in Table 1. Two main emission bands, peaked near 490 and 600 nm, are observed for both samples with excitation at 320 nm (coupled to 430 nm long-pass filter before the detector). For the InGaN/GaN NWs, the blue PL band (denoted as PL_1) at λ_{max} = 482 nm (~2.57 eV) can be attributed to recombination between the conduction band (CB) electron to valence band (VB) hole of the InGaN segments (In:Ga 2:8), which is consistent with the calculation results from density functional theory.[36] The longer wavelength and broad PL band (denoted as PL_2) peaked at 600 nm (~2.06 eV) is likely caused by charge-carrier recombination through shallow trap (ST) to deep acceptor (DA) states (Ga vacancy) in InGaN segments,[37,38] which is in good agreement with the defect (or yellow) emission from surface and interface defects along the growth axis of InGaN/GaN NWs reported previously.[39−42] The PLE spectrum of InGaN/GaN NWs shows strong absorption from 350 to 450 nm, consistent with previous reports.[15,39] The absorption features from 350 to 375 nm and 375−450 nm can be assigned as the electronic transition from VB to CB of the GaN (~3.4 eV) and the InGaN segments, respectively.

After the nonpolar surface of the InGaN/GaN NWs was decorated with Rh/Cr_2O_3 NPs, the similar PL emission peaks ($PL_{1'}$ and $PL_{2'}$) were observed as compared to pristine NWs (PL_1 and PL_2) without the Rh/Cr_2O_3 NP decoration, and the PLE feature of the InGaN/GaN-Rh/Cr_2O_3 NWs is still similar

DOI: 10.1021/acs.jpclett.5b00909
J. Phys. Chem. Lett. 2015, 6, 2649−2656

Table 1. Optical Properties of (a) InGaN/GaN and (b) InGaN/GaN−Rh/Cr_2O_3 NWs

absorption wavelength	PL1 wavelength	PL2 wavelength	PL2/PL1
350−357 nm (VB→CB, electronic transition of GaN)	λ_{max} = 482 nm (CB→VB, electron−hole recombination)	λ_{max} = 600 nm (ST→DA, electron−hole recombination through defect states)	0.83 of InGaN/GaN NWs
375−500 nm (VB→CB, electronic transition of InGaN)			0.67 of InGaN/GaN-Rh/Cr_2O_3 NWs

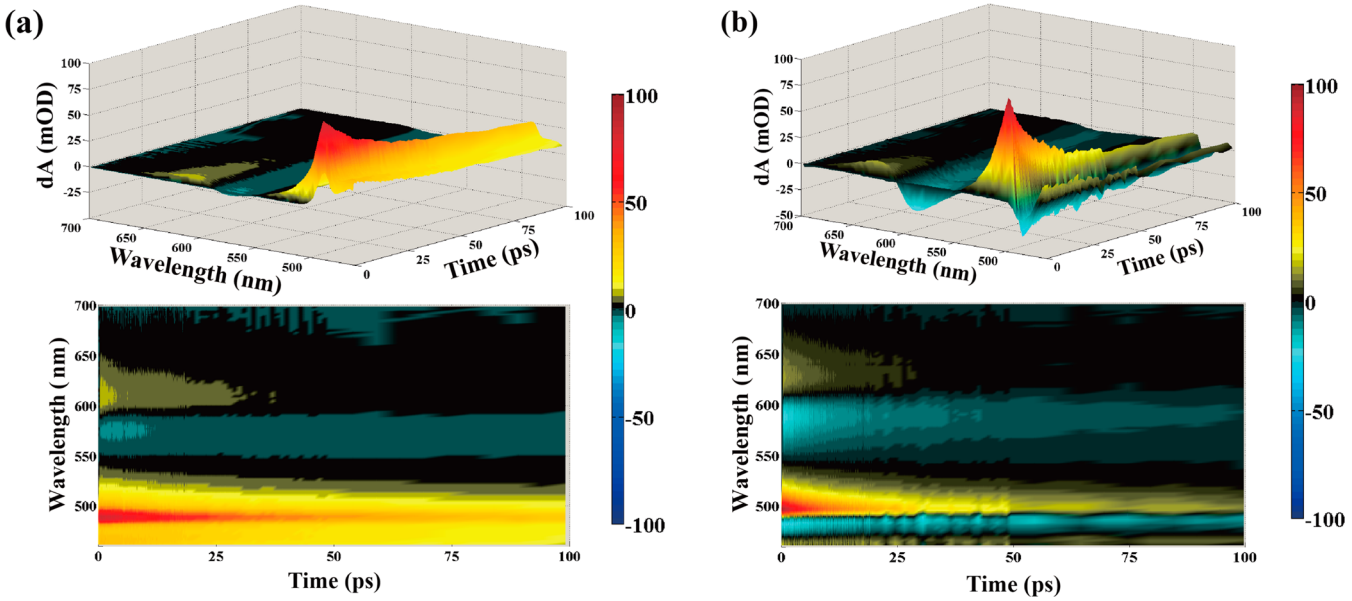

Figure 3. 3D and 2D transient absorption differential absorption spectrum of (a) InGaN/GaN NW and (b) InGaN/GaN-Rh/Cr_2O_3 NW at probe wavelength spanning 460−700 nm following at 415 nm, 93 nJ/pulse pump (1.1 mW/cm^2).

to InGaN/GaN NWs; however, the overall PL emission intensity of the InGaN/GaN-Rh/Cr_2O_3 NWs is lower than that of the InGaN/GaN NWs.[27] In addition, after the normalization of both PL spectra, the PL intensity ratio of defect emission ($PL_{2'}/PL_{1'}$) of the InGaN/GaN-Rh/Cr_2O_3 NWs is lower than that of the InGaN/GaN NWs (PL_2/PL_1). These results indicate that the decoration of Rh/Cr_2O_3 NPs on InGaN/GaN NWs reduced radiative exciton recombination through the surface defects and electron transfer from Rh/Cr_2O_3 NPs to InGaN/GaN NWs. The reduced contribution of the defect emission in the InGaN/GaN-Rh/Cr_2O_3 NWs may be attributed to the surface passivation by Rh/Cr_2O_3 NPs, which reduces the contribution of surface-state mediate recombination.[43,44] Meanwhile, the Rh/Cr_2O_3 NPs have also been reported as a role in extracting photoexcited electrons from the CB of semiconductors, leading to enhanced charge separation to inhibit electron−hole recombination, such as ($Ga_{1-x}Zn_x$)($N_{1-x}O_x$)-Rh/Cr_2O_3.[45−47] It is difficult to distinguish the two possible mechanisms using the PL results, which motivates us to further study their charge-carrier dynamics by femtosecond transient absorption (TA) techniques.

The TA spectra of InGaN/GaN and InGaN/GaN-Rh/Cr_2O_3 NWs were recorded by using 415 nm pump (pulse energy of 93 nJ/pulse, 1.1 mW/cm^2) and white-light probe (450−700 nm) as a function of time delay between the pump and probe pulses. We have also performed TA measurements using 350 nm pump and white-light probe, and we obtained similar results as that with 415 nm pump (SI, Figure S1). Because the InGaN/GaN and InGaN/GaN-Rh/Cr_2O_3 NWs are of interest for visible-light photocatalytic water splitting,[27] we choose to focus our analysis and discussion on the TA results using visible-light pump. The wavelength-dependent transient absorption (TA, excited-state absorption) and transient bleach (TB, ground-state depletion) profiles of InGaN/GaN and InGaN/GaN-Rh/Cr_2O_3 NWs were displayed as 3D and 2D plots in Figure 3a,b. Note that the chosen pump wavelength at 415 nm is only exciting the InGaN segments. The obtained signal of the InGaN/GaN NWs shows a sharp and asymmetrical TA feature with λ_{max} = 490 nm, a broad TB feature from 550 to 600 nm, and another broad TA feature from 600 to 650 nm. The time profile of the sharp 490 nm TA can be fit with a double exponential with a large amplitude fast decay of ∼17 ps and a smaller amplitude slow decay of ∼200 ps. The broad TB from 550 to 600 nm can be fit with a double exponential with a fast ∼7 ps and a slow ∼200 ps recovery. The longer wavelength and broad TA from 600 to 650 nm can be fit with a double exponential with a fast decay ∼2 ps and slow ∼60 ps decay. The sharp TA at 490 nm is likely a result of the electron absorption from CB (first excited state) to second excited state of InGaN segments, which illustrates the energy gap between CB and the second excited state is ∼2.5 eV (490 nm). The broad TA at 600−650 nm is attributed to electron absorption in the CB, while the TB feature at 550−600 nm is attributed to hole absorption in the VB of InGaN segments.

After Rh/Cr_2O_3 NPs are deposited on the surface of the InGaN/GaN NWs, the TA spectrum exhibits overall similar features as compared with that of undecorated InGaN/GaN NWs but has some differences. The TA spectrum of InGaN/GaN-Rh/Cr_2O_3 NWs shows a sharp and unsymmetrical TA band peaked at λ_{max} = 500 nm, a sharp and a broad TB feature at 450 to 470 nm and 550 to 610 nm, and another broad TA feature from 610 to 660 nm. The time profile of the sharp 500 nm TA feature can be fit with a double-exponential decay with a fast ∼11 ps decay and a slow ∼110 ps decay. The time profile

DOI: 10.1021/acs.jpclett.5b00909
J. Phys. Chem. Lett. 2015, 6, 2649−2656

of the sharp TB feature at λ_{max} = 485 nm can be fit with a double-exponential decay with a fast ∼12 ps and a slow ∼230 ps recovery. The broad TB at 550 to 610 nm can be fit with a double-exponential decay with a fast ∼6.5 ps and a slow ∼51 ps exponential recovery. The longer wavelength and broad TA at 610 to 660 nm can be fit with a double-exponential decay with a fast ∼2 ps and a slow ∼24 ps exponential decay. The sharp TA at 500 nm (∼2.48 eV) also resulted from the electron transition from CB to the second excited state of InGaN segments.

In addition, the broad TA at 610−660 nm is also attributed to the electron absorption in the CB of InGaN segments. Both of the TB features at 450−470 and 550−610 nm are attributed to hole absorption in the VB of InGaN segments. On the contrary, the dynamics signal showed a faster TA decay at 500 and 610−660 nm but slower TB recovery at 450−470 and 550−610 nm of InGaN/GaN-Rh/Cr_2O_3 NWs as compared with InGaN/GaN NWs. The shorter liftetime of photoexcited electrons at the CB but longer lifetime of photoexcited holes at the VB of InGaN/GaN-Rh/Cr_2O_3 NWs illustrates that the decorated Rh/Cr_2O_3 NPs play a role in extracting photoexcited electrons from the CB and leave the holes at the VB of InGaN. This result also rules out the possibility of surface-state passivation by the Rh/Cr_2O_3 NPs because surface-state passivation is usually associated with a longer lifetime of photoexcited electrons in the CB, for example, in core/shell/shell CdSe/ZnSe/ZnS and $Cd_{1-x}Zn_xSe$/ZnSe/ZnS quantum dots.[48,49] Therefore, the fitting results of TA signals confirmed that the decoration of Rh/Cr_2O_3 NPs on InGaN/GaN NWs can extract photoexcited electrons from the CB of InGaN, leading to better charge separation and longer-lived holes that are beneficial to photochemical water splitting. Moreover, the obtained TA results are consistent with the literature reporting that core/shell Rh/Cr_2O_3 NPs could extract photoexcited electrons from semiconductors to improve the efficiency of photocatalysis.[45,50,51]

The InGaN/GaN and InGaN/GaN-Rh/Cr_2O_3 NWs are expected to exhibit QW energy band structures, which are important for explaining the optical properties and exciton dynamics, as reflected in the TA/TB profiles shown in Figure 3. Although the TA/TB signals around 500−600 nm are stronger, they are mixed due to ground-state absorption of InGaN in this region, making it harder to analyze. At 650 nm, there is no ground-state electronic absorption and thus no TB signal, and the only TA signal is much easier to analyze. Figure 4a,b shows the TA decay profiles of InGaN/GaN and InGaN/GaN-Rh/Cr_2O_3 NWs at the probe wavelength of 625 nm under three different pump powers from 62, 93 to 167 nJ/pulse (0.7, 1.1, to 2.0 mW/cm^2). The TA decay traces can be fit with a triple-exponential function, and the fitting parameters are shown in Table 2. The amplitude of the fast decay component increased 1.2 and 1.5 times as the pump power increased from 62 to 93 (increase factor of 1.5) and 62 to 167 (increase factor of 2.7) nJ/pulse, respectively, of both InGaN/GaN and InGaN/GaN-Rh/Cr_2O_3 NWs. The linear behavior of the amplitude of the fast decay component was observed at lower pump power. On the contrary, the normalized TA decay profiles (Supporting Information, Figure S2) reveal power-dependent decay of both samples when the pump powers up to 167 nJ/pulse. The higher-order kinetic process can take place and result in faster decay or short lifetime, such as exciton−exciton annihilation or Auger recombination, with a lifetime of hundreds of femtoseconds to a few picoseconds.[52−57] The multiple excitons or

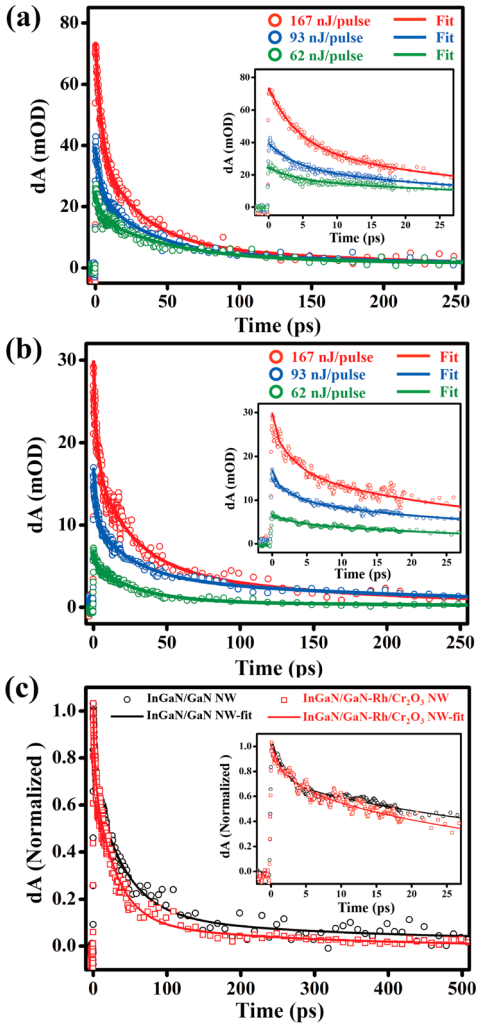

Figure 4. TA decay profile of (a) InGaN/GaN NWs and (b) InGaN/GaN−Rh/Cr_2O_3 NWs with pump power of 62, 93, and 167 nJ/pulse (0.7, 1.1, to 2.0 mW/cm^2). (c) Normalized TA decay profiles of InGaN/GaN and InGaN/GaN−Rh/Cr_2O_3 NWs with 62 nJ/pulse. Insets: TA profiles from 0 to 25 ps.

electron−hole pairs generated per NW could lead to saturation of the trap states. Upon the saturation of the trap states, additional excitons could accumulate and result in exciton−exciton annihilation, as reflected in power-dependent fast decay in the TA decay profiles. At low pump power, the power-independent decays and linear behaviors of both InGaN/GaN and InGaN/GaN-Rh/Cr_2O_3 NWs were observed, which illustrates that the excitons can dissociate into electrons and holes and then be trapped into trap states without saturation. To minimize the effect of higher-order and nonlinear processes, we focus our comparison on the results obtainable using the lowest possible power (62 nJ/pulse). The normalized TA decay profiles of InGaN/GaN and InGaN/GaN-Rh/Cr_2O_3 NWs that pumped with 62 nJ/pulse are shown in Figure 4c. In this case, the shorter average exciton lifetime of 164 ± 17 ps for InGaN/GaN-Rh/Cr_2O_3 NWs was observed as compared with the 247 ± 22 ps for InGaN/GaN NWs. On the fast time scale, both samples showed the similar decay behavior, while the larger amplitudes of medium and long time scale decay components were observed in InGaN/GaN-Rh/Cr_2O_3 NWs as compared with InGaN/GaN NWs. The shortened photoexcited electrons lifetime of InGaN/GaN-Rh/Cr_2O_3 NWs indicates that the

DOI: 10.1021/acs.jpclett.5b00909
J. Phys. Chem. Lett. 2015, 6, 2649−2656

Table 2. Summary of Exciton Lifetime from Triple Exponential Fitting of TA Data Probed at 625 nm for (a) InGaN/GaN and (b) InGaN/GaN−Rh/Cr_2O_3 NWs

(a)	A_1	τ_1 (ps)	A_2	τ_2 (ps)	A_3	τ_3 (ps)	<τ> (ps)
167 nJ	0.46 ± 0.02	4 ± 0.2	0.42 ± 0.02	29 ± 3	0.12 ± 0.02	213 ± 27	147 ± 24
93 nJ	0.38 ± 0.02	4 ± 0.3	0.50 ± 0.03	37 ± 5	0.12 ± 0.03	267 ± 26	178 ± 22
62 nJ	0.31 ± 0.03	4 ± 0.5	0.59 ± 0.04	50 ± 7	0.10 ± 0.02	400 ± 29	247 ± 22
(b)	A_1	τ_1 (ps)	A_2	τ_2 (ps)	A_3	τ_3 (ps)	<τ> (ps)
167 nJ	0.36 ± 0.04	3 ± 0.4	0.45 ± 0.07	25 ± 4	0.19 ± 0.01	132 ± 25	96 ± 14
93 nJ	0.28 ± 0.02	3 ± 0.2	0.56 ± 0.02	25 ± 3	0.16 ± 0.02	213 ± 23	156 ± 21
62 nJ	0.24 ± 0.02	3 ± 0.4	0.63 ± 0.06	29 ± 5	0.12 ± 0.02	250 ± 24	164 ± 17

decoration of Rh/Cr_2O_3 NP on InGaN/GaN NWs creates additional pathway for the photoexcited electrons to decay on the medium time scale, which could be injection of electrons from the CB of InGaN to Rh/Cr_2O_3 NPs.

To better understand the physical processes associated with the exciton and charge-carrier dynamics of the InGaN/GaN and InGaN/GaN-Rh/Cr_2O_3 NWs, we use a kinetic model as shown in Figure S3a in the SI to fit the observed TA/TB signals obtained at the lowest pump power (62 nJ/pulse).[56,58,59] The procedure for modeling and detail explanation are described in the SI. The proposed exciton relaxation processes of InGaN/GaN NWs involve the VB, CB, ST states, and DA states. The rate constants were adjusted iteratively and finally chosen based on best fit to the experimental results, similar to what has been done in the literature.[60−62] Because the TA signal contains contributions from different states, we need to account for that by summing up the modeled signals from relevant states. For example, by combining the contribution of 40% from both of the [VB] and the [CB] and 10% contribution of both the [ST] and the [DA] states, a curve could be generated that fit well with the experimental result of InGaN/GaN NWs. The final rate constants are determined when the modeled data match the experimental data. By this process, we are able to assign the time constants to the key physical process. For InGaN/GaN NWs, the time constant from the CB to the ST was modeled as 3 ps, while the decay from the ST to the DA was 25 ps, the CB to the DA was 33 ps, and the CB to the VB was 167 ps.

With decoration of Rh/Cr_2O_3 NPs on InGaN/GaN NWs, interfacial CT from the NWs to Rh/Cr_2O_3 NPs is expected. Therefore, we incorporate CT states in the kinetic model to fit the observed TA/TB signals of InGaN/GaN-Rh/Cr_2O_3 NWs, as shown in Figure S3a in the SI. To fit the experimental TA signals, we used 30% contribution of both the [VB] and the [CB], 30% contribution of [CT], and 5% contribution of both the [ST] and [DA]. The final rate constants were determined based on comparison of the modeled data and experimental data through several iterations. For Rh/Cr_2O_3-decorated NWs, the time constant from photoexcited electron decay from the CB to the ST was still modeled as 3 ps, the decay from the ST to the DA was 25 ps, the decay from the CB to the DA was 33 ps, and the decay from CB to the VB was 167 ps. More importantly, we obtained the time constant from the CB to the CT as 50 ps, which is uncovered only through the modeling process. In addition, the large contribution of [CT] indicates considerable electron transfer from the CB of InGaN/GaN NW to Rh/Cr_2O_3 NP, which is consistent with the observed PL decay in Figure 2.

The kinetic modeling is meant to provide a possible scheme to explain the TA/TB results and gain further insight beyond simple extraction of lifetimes from mathematical fitting. While the model is clearly not unique, it does highlight a possible scenario for the relaxation processes of the exciton or charge carriers in the InGaN/GaN and InGaN/GaN-Rh/Cr_2O_3 NWs.[63] The combined mathematical fitting and kinetic modeling led us to propose a general picture about the exciton relaxation processes in InGaN/GaN-Rh/Cr_2O_3 NWs, as shown in Figure 5. After the electron−hole pair is initially formed in

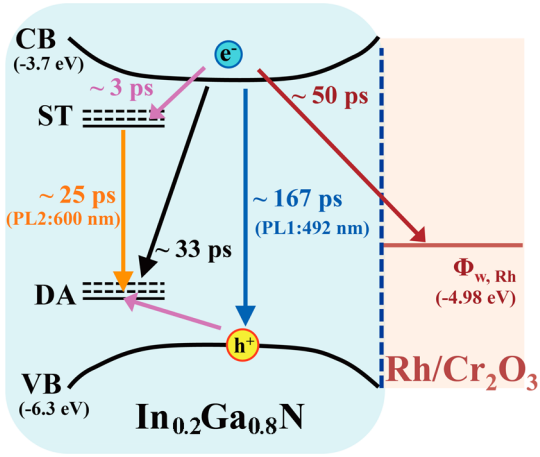

Figure 5. Scheme illustration of the exciton relaxation process in InGaN/GaN-Rh/Cr_2O_3 NWs, including band-edge energy of the CB and VB of $In_{0.2}Ga_{0.8}N$ and work function of Rh versus vacuum.

InGaN/GaN NWs, there are three major pathways for photoexcited electrons to relax in the InGaN segment. First, photoexcited electrons relax from the CB to ST states (~3 ps) and then into DA states (~25 ps). In parallel, photoexcited electrons can relax to DA states directly from the CB (~33 ps). In the meantime, the delocalized electrons at the CB can recombine with the hole at the VB, with a time constant of ~167 ps. Combining the results of PL studies with the proposed dynamics model of the InGaN/GaN NWs, we suggest that the relaxation processes from the CB to the ST are mostly nonradiative. The decays from the CB to DA and from ST to DA as well as from CB to VB are due to the combination of radiative and nonradiative decays. After the Rh/Cr_2O_3 NPs decorated on InGaN/GaN NWs, the photoexcited electron relaxation is similar to the undecorated NWs in lifetime except for the interfacial CT that takes place from the CB of the NWs to the CT state of Rh/Cr_2O_3 NPs (the work function of Rh ($\Phi_{w,Rh}$) is −4.98 eV vs vacuum[64]) in ~50 ps. The proposed dynamic model demonstrates that the decoration of Rh/Cr_2O_3 NPs on InGaN/GaN NWs results in better charge-separation properties, which is important for light-conversion applications.

The exciton and charge-carrier dynamics in InGaN/GaN and InGaN/GaN-Rh/Cr_2O_3 NWs have been studied by ultrafast TA pump−probe spectroscopy. The obtained TA features

DOI: 10.1021/acs.jpclett.5b00909
J. Phys. Chem. Lett. 2015, 6, 2649−2656

using the lowest pump power (62 nJ/pulse) at 625 nm were dominated by photoexcited exciton and charge-carrier relaxation that can be fit to a triple exponential with time constants of 4 ± 0.5, 50 ± 7, and 400 ± 29 ps and 3 ± 0.4, 29 ± 5, and 250 ± 24 ps for InGaN/GaN and InGaN/GaN-Rh/Cr_2O_3 NWs, respectively. The excitation power dependence shows linear behavior of the amplitudes of fast decay component under low pump power. Upon the high pump power, the fast decay component represents sublinear behavior due to high ordered exciton−exciton annihilation or Auger recombination upon trap-state saturation. Kinetic modeling of the experimental results provides further insight into the mechanisms of the exciton decay and charge-carrier relaxation. The modeled data for InGaN/GaN NWs demonstrate that the photoexcited electrons relaxation from the CB to the ST occurred with a time constant of 3 ps, while the ST-to-DA and CB-to-DA relaxation transition take place with a time constant of 25 and 33 ps, respectively. The electron−hole recombination from the CB to the VB, or exciton decay, occurred with a time constant of 167 ps. After decoration of Rh/Cr_2O_3 NPs onto the surface of InGaN/GaN NWs, a new decay pathway with a time constant of 50 ps was observed, which is attributed to interfacial CT from the CB of InGaN/GaN NWs to Rh/Cr_2O_3 NPs. The insight gained from the modeling about the relaxation processes of the exciton in such unique InGaN/GaN QW nanostructures is essential for further development for various applications, including solar energy conversion, photodetectors, LED, laser, and imaging.

■ ASSOCIATED CONTENT

Supporting Information

Methods, power dependence study, and details regarding the kinetic modeling of charge-carrier dynamics. The Supporting Information is available free of charge on the ACS Publications website at DOI: 10.1021/acs.jpclett.5b00909.

■ AUTHOR INFORMATION

Corresponding Authors

*E-mail: zhang@ucsc.edu (J.Z.Z.).
*E-mail: zetian.mi@mcgill.ca (Z.M.).

Notes

The authors declare no competing financial interest.

■ ACKNOWLEDGMENTS

This project was supported by the BES Division of the U.S. DOE and Delta Dental Health Associates. Part of the work was supported by the Natural Sciences and Engineering Research Council of Canada (NSERC) and the Climate Change and Emissions Management (CCEMC) Corporation. Part of the work was performed in the Microfabrication Facility at McGill University. Electron microscopy imaging and analysis were carried out at Facility for Electron Microscopy Research (FEMR), McGill University.

■ REFERENCES

(1) Qian, F.; Li, Y.; Gradecak, S.; Park, H. G.; Dong, Y.; Ding, Y.; Wang, Z. L.; Lieber, C. M. Multi-Quantum-Well Nanowire Heterostructures for Wavelength-Controlled Lasers. *Nat. Mater.* **2008**, *7*, 701−706.

(2) Qian, F.; Gradečak, S.; Li, Y.; Wen, C.-Y.; Lieber, C. M. Core-Multishell Nanowire Heterostructures as Multicolor High-Efficiency Light-Emitting Diodes. *Nano Lett.* **2005**, *5*, 2287−2291.

(3) Qian, F.; Li, Y.; Gradečak, S.; Wang, D.; Barrelet, C. J.; Lieber, C. M. Gallium Nitride-Based Nanowire Radial Heterostructures for Nanophotonics. *Nano Lett.* **2004**, *4*, 1975−1979.

(4) Ji, X.; Ma, J.; Wei, X.; Duan, R.; Wang, J.; Yi, X.; Zeng, Y.; Wang, G.; Yang, F.; Li, J. Investigation into Low-Temperature Photoluminescence Internal Quantum Efficiency and Defect-Recombination in InGaN Light-Emitting Diodes. *Phys. Status Solidi C* **2014**, *11*, 718−721.

(5) Kuykendall, T.; Ulrich, P.; Aloni, S.; Yang, P. Complete Composition Tunability of InGaN Nanowires Using a Combinatorial Approach. *Nat. Mater.* **2007**, *6*, 951−956.

(6) Zhao, S.; Kibria, M. G.; Wang, Q.; Nguyen, H. P.; Mi, Z. Growth of Large-Scale Vertically Aligned GaN Nanowires and their Heterostructures with High Uniformity on SiO_x by Catalyst-Free Molecular Beam Epitaxy. *Nanoscale* **2013**, *5*, 5283−5287.

(7) Pendyala, C.; Jasinski, J. B.; Kim, J. H.; Vendra, V. K.; Lisenkov, S.; Menon, M.; Sunkara, M. K. Nanowires as Semi-Rigid Substrates for Growth of Thick, $In_xGa_{1-x}N$ (x > 0.4) Epi-Layers without Phase Segregation for Photoelectrochemical Water Splitting. *Nanoscale* **2012**, *4*, 6269−6275.

(8) Fujii, K.; Kusakabe, K.; Ohkawa, K. Photoelectrochemical Properties of InGaN for H_2 Generation from Aqueous Water. *Jpn. J. Appl. Phys.* **2005**, *44*, 7433−7435.

(9) Aryal, K.; Pantha, B. N.; Li, J.; Lin, J. Y.; Jiang, H. X. Hydrogen Generation by Solar Water Splitting Using P-InGaN Photoelectrochemical Cells. *Appl. Phys. Lett.* **2010**, *96*, 052110.

(10) Caccamo, L.; Hartmann, J.; Fabrega, C.; Estrade, S.; Lilienkamp, G.; Prades, J. D.; Hoffmann, M. W.; Ledig, J.; Wagner, A.; Wang, X.; et al. Band Engineered Epitaxial 3D GaN-InGaN Core-Shell Rod Arrays as an Advanced Photoanode for Visible-Light-Driven Water Splitting. *ACS Appl. Mater. Interfaces* **2014**, *6*, 2235−2240.

(11) Benton, J.; Bai, J.; Wang, T. Utilisation of GaN and InGaN/GaN with Nanoporous Structures for Water Splitting. *Appl. Phys. Lett.* **2014**, *105*, 223902.

(12) Rajaambal, S.; Mapa, M.; Gopinath, C. S. $In_{1-x}Ga_xN$@ZnO: a Rationally Designed and Quantum Dot Integrated Material for Water Splitting and Solar Harvesting Applications. *Dalton Trans.* **2014**, *43*, 12546−12554.

(13) AlOtaibi, B.; Nguyen, H. P.; Zhao, S.; Kibria, M. G.; Fan, S.; Mi, Z. Highly Stable Photoelectrochemical Water Splitting and Hydrogen Generation Using a Double-Band InGaN/GaN Core/Shell Nanowire Photoanode. *Nano Lett.* **2013**, *13*, 4356−4361.

(14) Kibria, M. G.; Zhao, S.; Chowdhury, F. A.; Wang, Q.; Nguyen, H. P.; Trudeau, M. L.; Guo, H.; Mi, Z. Tuning the Surface Fermi Level on P-Type Gallium Nitride Nanowires for Efficient Overall Water Splitting. *Nat. Commun.* **2014**, *5*, 3825.

(15) Feng, S.-W.; Cheng, Y.-C.; Chung, Y.-Y.; Yang, C. C.; Lin, Y.-S.; Hsu, C.; Ma, K.-J.; Chyi, J.-I. Impact of Localized States on the Recombination Dynamics in InGaN/GaN Quantum Well Structures. *J. Appl. Phys.* **2002**, *92*, 4441.

(16) Badcock, T. J.; Dawson, P.; Davies, M. J.; Oliver, R. A.; Kappers, M. J.; Humphreys, C. J. Dynamics of Carrier Redistribution Processes in InGaN/GaN Quantum Well Structures. *Phys. Status Solidi C* **2014**, *11*, 738−741.

(17) Holmes, M. J.; Park, Y. S.; Wang, X.; Chan, C. C. S.; Jarjour, A. F.; Taylor, R. A.; Warner, J. H.; Luo, J.; El-Ella, H. A. R.; Oliver, R. A. Carrier Dynamics of $In_xGa_{1-x}N$ Quantum Disks Embedded in GaN Nanocolumns. *J. Appl. Phys.* **2011**, *109*, 063515.

(18) Jiang, B.; Zhang, C.; Wang, X.; Park, M. J.; Kwak, J. S.; Xu, J.; Zhang, H.; Zhang, J.; Xue, F.; Xiao, M. The Impact of Carrier Transport Confinement on the Energy Transfer Between InGaN/GaN Quantum-Well Nanorods and Colloidal Nanocrystals. *Adv. Funct. Mater.* **2012**, *22*, 3146−3152.

(19) Pu, Y.-C.; Chen, Y.-C.; Hsu, Y.-J. Au-Decorated $Na_xH_{2-x}Ti_3O_7$ Nanobelts Exhibiting Remarkable Photocatalytic Properties under Visible-Light Illumination. *Appl. Catal., B* **2010**, *97*, 389−397.

(20) Cheng, W.-Y.; Chen, W.-T.; Hsu, Y.-J.; Lu, S.-Y. Modulation and Improvement on Separation of Photoinduced Charge Carriers in CdS-

DOI: 10.1021/acs.jpclett.5b00909
J. Phys. Chem. Lett. 2015, 6, 2649−2656

Metal Nanoheterostructures. *J. Phys. Chem. C* **2009**, *113*, 17342−17346.
(21) Dasgupta, N. P.; Liu, C.; Andrews, S.; Prinz, F. B.; Yang, P. Atomic Layer Deposition of Platinum Catalysts on Nanowire Surfaces for Photoelectrochemical Water Reduction. *J. Am. Chem. Soc.* **2013**, *135*, 12932−12935.
(22) Yoshida, M.; Yamakata, A.; Takanabe, K.; Kubota, J.; Osawa, M.; Domen, K. ATR-SEIRAS Investigation of the Fermi Level of Pt Cocatalyst on a GaN Photocatalyst for Hydrogen Evolution under Irradiation. *J. Am. Chem. Soc.* **2009**, *131*, 13218−13219.
(23) Oh, I.; Kye, J.; Hwang, S. Enhanced Photoelectrochemical Hydrogen Production from Silicon Nanowire Array Photocathode. *Nano Lett.* **2012**, *12*, 298−302.
(24) Elmalem, E.; Saunders, A. E.; Costi, R.; Salant, A.; Banin, U. Growth of Photocatalytic CdSe-Pt Nanorods and Nanonets. *Adv. Mater.* **2008**, *20*, 4312−4317.
(25) Kibria, M. G.; Nguyen, H. P. T.; Cui, K.; Zhao, S.; Liu, D.; Guo, H.; Trudeau, M. L.; Paradis, S.; Hakima, A.-R.; Mi, Z. One-Step Overall Water Splitting under Visible Light Using Multiband InGaN-GaN Nanowire Heterostructures. *ACS Nano* **2013**, *7*, 7886−7893.
(26) Hisatomi, T.; Kubota, J.; Domen, K. Recent Advances in Semiconductors for Photocatalytic and Photoelectrochemical Water Splitting. *Chem. Soc. Rev.* **2014**, *43*, 7520−7535.
(27) Kibria, M. G.; Chowdhury, F. A.; Zhao, S.; AlOtaibi, B.; Trudeau, M. L.; Guo, H.; Mi, Z. Visible Light-Driven Efficient Overall Water Splitting Using P-Type Metal-Nitride Nanowire Arrays. *Nat. Commun.* **2015**, *6*, 6797.
(28) Pu, Y.-C.; Lin, W.-H.; Hsu, Y.-J. Modulation of Charge Carrier Dynamics of $Na_xH_{2-x}Ti_3O_7$-Au-Cu_2O Z-Scheme Nanoheterostructures through Size Effect. *Appl. Catal., B* **2015**, *163*, 343−351.
(29) Pu, Y.-C.; Ling, Y.; Chang, K.-D.; Liu, C.-M.; Zhang, J. Z.; Hsu, Y.-J.; Li, Y. Surface Passivation of TiO_2 Nanowires Using a Facile Precursor-Treatment Approach for Photoelectrochemical Water Oxidation. *J. Phys. Chem. C* **2014**, *118*, 15086−15094.
(30) Wheeler, D. A.; Ling, Y.; Dillon, R. J.; Fitzmorris, R. C.; Dudzik, C. G.; Zavodivker, L.; Rajh, T.; Dimitrijevic, N. M.; Millhauser, G.; Bardeen, C.; et al. Probing the Nature of Bandgap States in Hydrogen-Treated TiO_2 Nanowires. *J. Phys. Chem. C* **2013**, *117*, 26821−26830.
(31) Pesci, F. M.; Wang, G.; Klug, D. R.; Li, Y.; Cowan, A. J. Efficient Suppression of Electron-Hole Recombination in Oxygen-Deficient Hydrogen-Treated TiO_2 Nanowires for Photoelectrochemical Water Splitting. *J. Phys. Chem. C* **2013**, *117*, 25837−25844.
(32) Prasankumar, R. P.; Upadhya, P. C.; Taylor, A. J. Ultrafast Carrier Dynamics in Semiconductor Nanowires. *Phys. Status Solidi B* **2009**, *246*, 1973−1995.
(33) Fitzmorris, B. C.; Larsen, G. K.; Wheeler, D. A.; Zhao, Y.; Zhang, J. Z. Ultrafast Charge Transfer Dynamics in Polycrystalline CdSe/TiO_2 Nanorods Prepared by Oblique Angle Codeposition. *J. Phys. Chem. C* **2012**, *116*, 5033−5041.
(34) Larsen, G. K.; Fitzmorris, B. C.; Longo, C.; Zhang, J. Z.; Zhao, Y. Nanostructured Homogenous CdSe−TiO_2 Composite Visible Light Photoanodes Fabricated by Oblique Angle Codeposition. *J. Mater. Chem.* **2012**, *22*, 14205−14218.
(35) Li, J.; Cushing, S. K.; Zheng, P.; Senty, T.; Meng, F.; Bristow, A. D.; Manivannan, A.; Wu, N. Solar Hydrogen Generation by a CdS-Au-TiO_2 Sandwich Nanorod Array Enhanced with Au Nanoparticle as Electron Relay and Plasmonic Photosensitizer. *J. Am. Chem. Soc.* **2014**, *136*, 8438−8449.
(36) Moses, P. G.; Van de Walle, C. G. Band Bowing and Band Alignment in InGaN Alloys. *Appl. Phys. Lett.* **2010**, *96*, 021908.
(37) Sedhain, A.; Li, J.; Lin, J. Y.; Jiang, H. X. Nature of Deep Center Emissions in GaN. *Appl. Phys. Lett.* **2010**, *96*, 151902.
(38) Neugebauer, J. r.; Van de Walle, C. G. Gallium Vacancies and the Yellow Luminescence in GaN. *Appl. Phys. Lett.* **1996**, *69*, 503.
(39) Yang, F.; Zhang, C.; Shi, C.; Joo Park, M.; Seop Kwak, J.; Jung, S.; Choi, Y.-H.; Wu, X.; Wang, X.; Xiao, M. Defect Recombination Induced by Density-Activated Carrier Diffusion in Nonpolar InGaN Quantum Wells. *Appl. Phys. Lett.* **2013**, *103*, 123506.
(40) Manz, C.; Kunzer, M.; Obloh, H.; Ramakrishnan, A.; Kaufmann, U. $In_xGa_{1-x}N$/GaN Band Offsets as Inferred from the Deep, Yellow-Red Emission Band in $In_xGa_{1-x}N$. *Appl. Phys. Lett.* **1999**, *74*, 3993.
(41) Jeong, M. S.; Kim, Y. W.; White, J. O.; Suh, E. K.; Cheong, M. G.; Kim, C. S.; Hong, C. H.; Lee, H. J. Spatial Variation of Photoluminescence and Related Defects in InGaN/GaN Quantum Wells. *Appl. Phys. Lett.* **2001**, *79*, 3440.
(42) Jeon, E. S.; Kozlov, V.; Song, Y. K.; Vertikov, A.; Kuball, M.; Nurmikko, A. V.; Liu, H.; Chen, C.; Kern, R. S.; Kuo, C. P.; et al. Recombination Dynamics in InGaN Quantum Wells. *Appl. Phys. Lett.* **1996**, *69*, 4194.
(43) Pu, Y.-C.; Wang, G.; Chang, K.-D.; Ling, Y.; Lin, Y.-K.; Fitzmorris, B. C.; Liu, C.-M.; Lu, X.; Tong, Y.; Zhang, J. Z.; et al. Au Nanostructure-Decorated TiO_2 Nanowires Exhibiting Photoactivity Across Entire UV-Visible Region for Photoelectrochemical Water Splitting. *Nano Lett.* **2013**, *13*, 3817−3823.
(44) Chen, T.; Xing, G. Z.; Zhang, Z.; Chen, H. Y.; Wu, T. Tailoring the Photoluminescence of ZnO Nanowires Using Au Nanoparticles. *Nanotechnology* **2008**, *19*, 435711.
(45) Ikeda, T.; Xiong, A.; Yoshinaga, T.; Maeda, K.; Domen, K.; Teranishi, T. Polyol Synthesis of Size-Controlled Rh Nanoparticles and their Application to Photocatalytic Overall Water Splitting under Visible Light. *J. Phys. Chem. C* **2013**, *117*, 2467−2473.
(46) Maeda, K.; Teramura, K.; Lu, D.; Saito, N.; Inoue, Y.; Domen, K. Roles of Rh-Cr_2O_3 Core-Shell Nanoparticles Photodeposited on Visible-Light Responsive $Ga_{1-x}Zn_xN_{1-x}O_x$ Solid Solutions in Photocatalytic Overall Water Splitting. *J. Phys. Chem. C* **2007**, *111*, 7554−7560.
(47) Dixon, E. Some Photoelectric and Thermionic Properties of Rhodium. *Phys. Rev.* **1931**, *37*, 60−69.
(48) Fitzmorris, B. C.; Pu, Y.-C.; Cooper, J. K.; Lin, Y.-F.; Hsu, Y.-J.; Li, Y.; Zhang, J. Z. Optical Properties and Exciton Dynamics of Alloyed Core/Shell/Shell $Cd_{1-x}Zn_xSe$/ZnSe/ZnS Quantum Dots. *ACS Appl. Mater. Interfaces* **2013**, *5*, 2893−900.
(49) Fitzmorris, B. C.; Cooper, J. K.; Edberg, J.; Gul, S.; Guo, J.; Zhang, J. Z. Synthesis and Structural, Optical, and Dynamic Properties of Core/Shell/Shell CdSe/ZnSe/ZnS Quantum Dots. *J. Phys. Chem. C* **2012**, *116*, 25065−25073.
(50) Maeda, K.; Sakamoto, N.; Ikeda, T.; Ohtsuka, H.; Xiong, A.; Lu, D.; Kanehara, M.; Teranishi, T.; Domen, K. Preparation of Core-Shell-Structured Nanoparticles (with a Noble-Metal or Metal Oxide Core and a Chromia Shell) and their Application in Water Splitting by Means of Visible Light. *Chem.—Eur. J.* **2010**, *16*, 7750−7759.
(51) Yoshida, M.; Takanabe, K.; Maeda, K.; Ishikawa, A.; Kubota, J.; Sakata, Y.; Ikezawa, Y.; Domen, K. Role and Function of Noble-Metal Cr Layer Core-Shell Structure Cocatalysts for Photocatalytic Overall Water Splitting Studied by Model Electrodes. *J. Phys. Chem. C* **2009**, *113*, 10151−10157.
(52) Roberti, T. W.; Cherepy, N. J.; Zhang, J. Z. Nature of the Power-Dependent Ultrafast Relaxation Process of Photoexcited Charge Carriers in II-VI Semiconductor Quantum Dots: Effects of Particle Size, Surface, and Electronic Structure. *J. Chem. Phys.* **1998**, *108*, 2143.
(53) Zheng, J. P.; Kwok, H. S. Exciton and Biexciton Recombination in Semiconductor Nanocrystals. *Appl. Phys. Lett.* **1994**, *65*, 1151.
(54) Burda, C.; Link, S.; Mohamed, M. B.; El-Sayed, M. The Pump Power Dependence of the Femtosecond Relaxation of CdSe Nanoparticles Observed in the Spectral Range from Visible to Infrared. *J. Chem. Phys.* **2002**, *116*, 3828.
(55) Burda, C.; Link, S.; Green, T. C.; El-Sayed, M. A. New Transient Absorption Observed in the Spectrum of Colloidal CdSe Nanoparticles Pumped with High-Power Femtosecond Pulses. *J. Phys. Chem. B* **1999**, *103*, 10775−10780.
(56) Wheeler, D. A.; Huang, J.-A.; Newhouse, R. J.; Zhang, W.-F.; Lee, S.-T.; Zhang, J. Z. Ultrafast Exciton Dynamics in Silicon Nanowires. *J. Phys. Chem. Lett.* **2012**, *3*, 766−771.
(57) Xu, X.; Zhao, Y.; Sie, E. J.; Lu, B.; Liu, B.; Ekahana, S. A.; Ju, X.; Jiang, Q.; Wang, J.; Sun, H.; et al. Dynamics of Bound Exciton Complexes in CdS Nanobelts. *ACS Nano* **2011**, *5*, 3660−3669.

DOI: 10.1021/acs.jpclett.5b00909
J. Phys. Chem. Lett. 2015, 6, 2649−2656

(58) Brelle, M. C.; Zhang, J. Z. Femtosecond Study of Photo-Induced Electron Dynamics in AgI and Core/Shell Structured AgI/Ag_2S and AgBr/Ag_2S Colloidal Nanoparticles. *J. Chem. Phys.* **1998**, *108*, 3119.
(59) Brelle, M. C.; Torres-Martinez, C. L.; McNulty, J. C.; Mehra, R. K.; Zhang, J. Z. Synthesis and Characterization of Cu_xS Nanoparticles Nature of the Infrared Band and Charge-Carrier Dynamics. *Pure Appl. Chem.* **2000**, *72*, 101−117.
(60) Shin, T.; Li, X.-S.; Ko, D.-S.; Won, J.-Y.; Kim, S.-H.; Kim, J.; Kim, J.; Tak, Y.; Kim, J.-Y.; Park, G.-S.; et al. Photocarrier Dynamics Near V-Shaped Pits in $In_xGa_{1-x}N$/GaN Multiple Quantum Wells. *Chem. Phys.* **2014**, *436*−*437*, 51−54.
(61) Sun, C. K.; Vallée, F.; Keller, S.; Bowers, J. E.; DenBaars, S. P. Femtosecond Studies of Carrier Dynamics in InGaN. *Appl. Phys. Lett.* **1997**, *70*, 2004.
(62) Omae, K.; Kawakami, Y.; Fujita, S.; Narukawa, Y.; Mukai, T. Effects of Internal Electrical Field on Transient Absorption in $In_xGa_{1-x}N$ Thin Layers and Quantum Wells with Different Thickness by Pump and Probe Spectroscopy. *Phys. Rev. B* **2003**, *68*, 085303.
(63) Wheeler, D. A.; Zhang, J. Z. Exciton Dynamics in Semiconductor Nanocrystals. *Adv. Mater.* **2013**, *25*, 2878−2896.
(64) Dixon, E. H. Some Photoelectric and Thermionic Properties of Rhodium. *Phys. Rev.* **1931**, *37*, 60−69.

DOI: 10.1021/acs.jpclett.5b00909
J. Phys. Chem. Lett. 2015, 6, 2649−2656